
01 Jan 2023

Effects of Molecular Size and Orientation on the Interfacial Properties and Wetting Behavior of Water/ N -Alkane Systems: A Molecular-Dynamics Study

Fawaz Hrahsheh

Gerald Wilemski

Missouri University of Science and Technology, wilemski@mst.edu

Follow this and additional works at: https://scholarsmine.mst.edu/phys_facwork

 Part of the [Physics Commons](#)

Recommended Citation

F. Hrahsheh and G. Wilemski, "Effects of Molecular Size and Orientation on the Interfacial Properties and Wetting Behavior of Water/ N -Alkane Systems: A Molecular-Dynamics Study," *Physical Chemistry Chemical Physics*, Royal Society of Chemistry, Jan 2023.



The definitive version is available at <https://doi.org/10.1039/d2cp05735b>

This Article - Journal is brought to you for free and open access by Scholars' Mine. It has been accepted for inclusion in Physics Faculty Research & Creative Works by an authorized administrator of Scholars' Mine. This work is protected by U. S. Copyright Law. Unauthorized use including reproduction for redistribution requires the permission of the copyright holder. For more information, please contact scholarsmine@mst.edu.



Cite this: *Phys. Chem. Chem. Phys.*, 2023, 25, 5808

Effects of molecular size and orientation on the interfacial properties and wetting behavior of water/*n*-alkane systems: a molecular-dynamics study†

Fawaz Hrahsheh *^a and Gerald Wilemski ^b

Molecular dynamics simulations (MD) are performed to study the interfacial structure/tension and wetting behavior of water/*n*-alkane systems (water/*n*C5 to water/*n*C16 where $nC_x = C_xH(2x + 2)$). In particular, we study complete-to-partial wetting transitions by changing the *n*-alkane chain length (N_C) at a constant temperature, $T = 295$ K. Simulations are carried out with a united-atom TraPPE model for *n*-alkanes and the TIP4P-2005 model of water. Simulation results are in excellent agreement with the initial spreading coefficients and contact angles calculated using experimental values of the surface and interfacial tensions. In addition, it has been determined that water/(*n*C5–*n*C7) and water/(*n*C8–*n*C16), respectively, exhibit complete and partial initial wetting modes. Simulations show that the interfacial structures of water/(*n*C5–*n*C7) are different from water/(*n*C8–*n*C16) systems. In the latter, water preferentially orients near the interface to increase the number of hydrogen bonds and the charge and mass densities. Moreover, the orientation of *n*-alkane molecules at water/(*n*C8–*n*C16) interfaces has a long-range persistence, resulting in layered structures that increase with N_C . In addition, simulation results of the orientational order parameter S_z show alignment behavior of the *n*-alkane molecules with respect to the interfaces. Simulations predict that the central segments of *n*-alkane are strongly packed in the interfaces while the end segments (methyl groups) form smaller peaks in the outer edge of the layer. This observation confirms the “horseshoe” or “C-shaped” structure of *n*-alkane molecules in the water/*n*-alkane interfaces. At constant temperature, the interface widths of both water and the *n*-alkanes decrease with increasing *n*-alkane molecular length. These results suggest that increasing the *n*-alkane chain length affects the water/*n*-alkane interfacial properties in a manner similar to that of cooling.

Received 8th December 2022,
Accepted 26th January 2023

DOI: 10.1039/d2cp05735b

rsc.li/pccp

1 Introduction

Many investigations have been performed to study aqueous/organic interfaces because of their relevance in environmental and industrial applications. Alkanes are organic molecules that are used extensively to study such interfaces because of their simple chain structure. Moreover, they form the main building blocks of more complex organic compounds.^{1–7} Similar to the mutual solubility of water/organic mixtures, wetting behavior is a key feature in the field of aqueous/organic interfaces. In general, the degree of wetting, *i.e.*, partial or complete, will be determined by the balance of surface free energies of the

materials involved. The surface free energy is the excess energy that the surface has compared with the bulk phase of the material. In the bulk, because of isotropy and symmetry, molecules experience a zero-net force on average. By contrast, interfaces are inherently anisotropic and inhomogeneous, and this loss of symmetry results in the surface free energy. The magnitude of the surface free energy depends on the interactions between the molecules. In the case of water, the surface free energy is high due to strong hydrogen bonds and dipole–dipole interactions between the water molecules. In *n*-alkanes, the molecular forces are typically much weaker, and thus the surface free energy of *n*-alkanes is low.

For decades, *n*-alkane systems (particularly pentane, hexane, and heptane) have been theoretically and experimentally studied to determine whether or not they spread over water under ambient conditions.^{8–18} Because many of the results were contradictory, it has been difficult to reach a consensus on the equilibrium wetting behavior. Subsequent work has established a more consistent picture in which pentane and all longer *n*-alkanes do not wet water at room temperature.^{14,17,19–22}

^a Higher Colleges of Technology, ETS, MZWC, Abu Dhabi, 58855,

United Arab Emirates. E-mail: fhrhsheh@hct.ac.ae, fyh44f@umsystem.edu

^b Department of Physics, Missouri University of Science and Technology, Rolla, MO 65409, USA. E-mail: wilemski@mst.edu

† Electronic supplementary information (ESI) available. See DOI: <https://doi.org/10.1039/d2cp05735b>

In this work, we study water/*n*-alkane interfacial properties, particularly the initial wetting behavior, using molecular-dynamics simulations. Because it is not easy to calculate the surface free energy, water/*n*-alkane wetting is usually determined *via* an equivalent property, the interfacial tension. For complete wetting, the water–vapor surface tension (γ_{wv}) exceeds the sum of the water–alkane (γ_{wa}) and alkane–vapor (γ_{av}) surface tensions ($\gamma_{\text{wv}} > \gamma_{\text{wa}} + \gamma_{\text{av}}$), while for partial wetting, the water–vapor surface tension is smaller than these combined surface tensions ($\gamma_{\text{wv}} < \gamma_{\text{wa}} + \gamma_{\text{av}}$). According to Rowlinson and Widom,²³ these inequality formulas are actually equivalent to the so-called spreading coefficient,

$$S = \gamma_{\text{wv}} - (\gamma_{\text{wa}} + \gamma_{\text{av}}), \quad (1)$$

which must be negative to fulfill the condition for equilibrium of three phases at a line of mutual contact. Transitions between the complete and partial wetting of oil on water can occur, induced by the variation of several parameters including, but not limited to, a changing temperature,²⁴ tuning the mutual interactions,²⁵ and adding salt/surfactants.^{5,26,27}

From molecular simulations, the average surface tension γ is readily calculated from the difference between normal and lateral values of the pressure as follows:²⁸

$$\gamma = \frac{L_z}{2} [\langle P_n \rangle - \langle P_t \rangle] \quad (2)$$

where L_z is the length of the simulation box normal to the interface, and $\langle P_n \rangle$ and $\langle P_t \rangle$ are, respectively, the mean pressure tensors normal (z) and tangential (xy) to the interface. They are averaged over 150 ns of *NVT* simulations after 10 ns of equilibration.

To assess the reliability of our simulations, we compare our results for the spreading coefficients and contact angles with calculations based on the experimental data of Goebel and Lunkenheimer.^{1,29} These researchers carried out several purification cycles to determine the water/oil interfacial tensions using the ring method, with accuracies reaching $\pm 0.2\%$ at 295 K. We also compare our results with the measurements of Zepfieri *et al.*²

In this work, we use equilibrium molecular dynamic simulations to study water/*n*-alkane interfaces at a constant temperature, $T = 295$ K. Fixing the simulation temperature enables us to investigate the effects of the *n*-alkane chain length N_C on the wetting behavior. Here, we denote *n*-alkanes symbolically as *nCx*, such as *nC5* for normal-pentane and *nC16* for normal-hexadecane. In addition to the spreading coefficient S , we calculate the water/*nCx* contact angles, θ_c , using a rigorously derived formula,²³

$$\cos(\theta_c) = \frac{\gamma_{\text{wv}}^2 - \gamma_{\text{wa}}^2 - \gamma_{\text{av}}^2}{2\gamma_{\text{wa}}\gamma_{\text{av}}}. \quad (3)$$

To calculate the spreading coefficients and contact angles using eqn (1) and (3), we determine the interfacial tensions of pure water/vapor, pure *nCx*/vapor, and water/*nCx* at $T = 295$ K.‡

We monitor the *n*-alkane chain orientation in the interfaces using an orientational order parameter S_z defined in terms of

the angle ϕ between the interface normal vector (the director) and some vector describing the local orientation of the molecule. The vector connecting a pair of carbon atoms that are two units apart in a molecule (*e.g.*, atoms 1 and 3) is found to be a convenient vector for this parameter.^{30,31} This order parameter is actually the second Legendre polynomial of $\cos(\phi)$ averaged over all vectors and time steps. Thus, it is defined as:

$$S_z = \frac{3\langle \cos^2(\phi) \rangle - 1}{2}. \quad (4)$$

The order parameter S_z provides a convenient quantification of the alignment: $S_z = 1$ denotes perfect alignment (along the director), $0 < S_z < 1$ denotes partial alignment, $S_z = 0$ denotes a completely random alignment, and $S_z = -1/2$ denotes completely perpendicular-alignment to the director.

2 Methods and simulation settings

Two united-atom (UA) force fields are initially used to model the *n*-alkanes: PYS (Paul, Yoon, Smith)^{32–34} and TraPPE (Transferable Potentials for Phase Equilibria).^{35–38} These united-atom force fields have been used widely to study the thermodynamic properties of alkanes, including phase-equilibria, interfacial properties, and phase transitions.^{24,39–47} Water is modeled with a rigid four-site model TIP4P-2005, which consists of three fixed point charges (two hydrogen atoms HW1 and HW2, and one virtual site M) and one Lennard-Jones center (a neutral oxygen atom O).⁴⁸ The surface tension of the TIP4P-2005 model has been studied using several methods that confirm the validity and reliability of this model.^{49–52} One of the main differences between the PYS and TraPPE models is that the PYS model assumes that both methyl and methylene groups interact identically with water.

The molecular dynamics simulations in this work were performed using the GROMACS software package.^{53–56} The classical equations of motions are integrated with the velocity Verlet algorithm⁵⁷ with a time-step of 5 fs. § We use periodic simulation cells in the three directions and we control the temperature using the v-rescale thermostat⁵⁸ with a time constant of 0.2 ps. A fast and stable algorithm (LINC algorithm) is used to maintain the water molecule rigidity.⁵⁹ The electrostatic interactions were implemented using a particle-mesh Ewald method.⁶⁰ All the *nC*–*nC*, water–water, and water–*nC* interactions are cut-off at 1.5 nm. Although the long-range van der Waals tail corrections to the energy and pressure are accurate for homogeneous systems with a long cut-off, they do not directly treat the properties of inhomogeneous systems such as interfacial tensions.⁶¹ For such cases, a variant of the particle mesh Ewald algorithm had already been proposed for the Lennard-Jones dispersion interactions (LJ-PME),⁶² but it was

‡ Using the LJ-PME enables us to use a larger timestep (5 fs) with $r_c = 1.5$ nm. Our surface tension results agree with the results of Neupane and Wilemski's study (ESI),²⁴ in which they implemented the LJ potential using the cut-off method with a long cut-off radius $r_c = 2.4$ nm and a 1 fs timestep, and included the long-range tail correction.

‡ As discussed elsewhere,²⁴ only initial spreading coefficients and contact angles are determined here, but for simplicity we omit repeating the word "initial".

implemented only recently in GROMACS.⁶³ This method is used here, and it enables the surface tensions of liquids as well as bulk properties, such as density, to be determined without approximations due to truncation.^{61,64,65}

In this work, MD simulations of water/*n*-alkane systems are performed for one slab of water placed between two slabs of *n*-alkane. In addition to the temperature, we fix the number of molecules and the simulation box volume in *NVT* simulations. Therefore, increasing the *n*-alkane chain length decreases the vapor-to-liquid volume ratio. This occurrence leads to significant effects on the simulation conditions (and hence the system pressure, liquid–vapor equilibrium, and interfacial tensions). To keep the *NVT* conditions the same for all water/*n*-alkane simulations, we fix the number of carbon atoms for all *n*-alkanes instead of the number of molecules. We begin with the longest *n*-alkane chain in our study (*n*C16) because it needs simulation slabs to be thick enough to avoid any correlation between its *n*C16/vapor and water/*n*C16 interfaces. We find that 2400 carbon atoms and 1500 water molecules in $3.5 \times 3.5 \times 25$ nm is sufficient to achieve isotropic bulk phases for all *n*-alkane systems in our study (*n*C5–*n*C16). The vapor phase in the *Z* direction is thick enough so that the two *n*-alkane/vapor interfaces do not interact with each other even though periodic boundary conditions are imposed. The MD simulations of pure *n*-alkane and water are performed with the same number of molecules in the corresponding water/*n*-alkane systems and in simulation boxes three times larger than the liquid thickness, $5 \times 5 \times 15$ nm.

3 Results and discussion

To compare with the measurements of interfacial tensions by Goebel and Lunkenheimer¹ at $T = 295$ K, we calculated the interfacial tension of a set of *n*-alkane systems using two different models (PYS and TraPPE). As shown in Fig. 1, the dependence of the PYS surface tension on N_C is very high

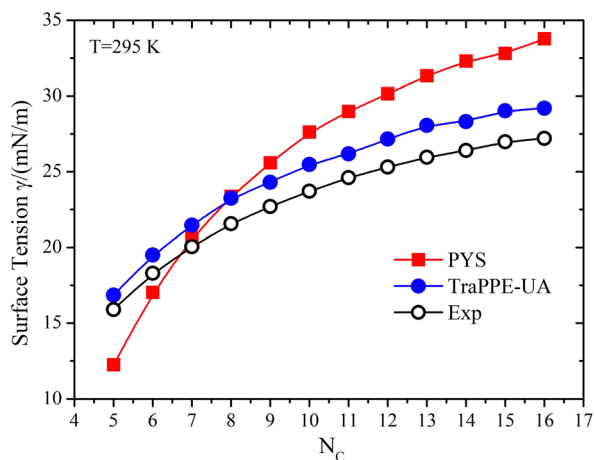


Fig. 1 Chain length (N_C) dependence of the surface tension plotted for *n*-alkanes: PYS (squares) and TraPPE-UA (filled circles) are compared with the surface tension values (open circles) of Goebel and Lunkenheimer.¹ All of the standard errors of the mean are smaller than the marker size, and are not shown here. A table that includes these values is provided in the ESI.†

compared with the experimental values.¹ Thus, using the PYS force field requires a separate tuning of the water/*n*-alkane interaction strength ϵ_{OC} for each *n*-alkane, which is very expensive computationally. This behavior of the surface tension for the PYS model needs more investigation, particularly regarding its effect on the interfaces.

To avoid this complication, we decided to use the TraPPE-UA force field in modeling our *n*-alkane systems. The surface tension values of the *n*-alkanes using the TraPPE-UA model agree fairly well with the experimental values (Fig. 1) in both magnitude and the rate of change with N_C .¹

To further confirm the reliability of the TraPPE-UA model, we determined the bulk densities for *n*-alkanes and compared them with results extracted from the empirical formula of Olabisi and Simha,^{66,67} as shown in Fig. 2. Our results for the *n*-alkane bulk densities show a very good agreement with the calculations of their empirical equation.

The good behavior of the TraPPE-UA pure alkane results enables us to tune the water/*n*-alkane interaction strengths for only one *n*-alkane system and then use the resultant parameters for the other *n*-alkanes. Since the spreading coefficient and contact angles do not depend on the magnitudes of surface tension themselves but on the differences shown in eqn (1) and (3), we need to tune only the water/*n*-alkane interaction parameters. The strength of the interaction between TIP4P-2005 and TraPPE-UA (ϵ_{OC}) is tuned for heptane (*n*C7) at $T = 295$ K. Heptane (*n*C7) is chosen because its experimental initial spreading coefficient¹ ($S_{\text{exp}} = 0.57$) is fairly close to the transition value, $S = 0$, at $T = 295$ K. Our tuning parameter r is defined in terms of the Lorentz–Berthelot combining rules as $\epsilon_{OC} = (1 + r)\sqrt{\epsilon_O\epsilon_C}$, where ϵ_O and ϵ_C are the O–O and *n*C–*n*C interactions, respectively.^{68,69} The optimal strength of interaction between the TIP4P-2005 oxygen atom and the TraPPE methyl/methylene groups is found at $r = 0.12$. Therefore, the new interaction strengths of water/*n*-alkane ϵ_{OC} for the methyl

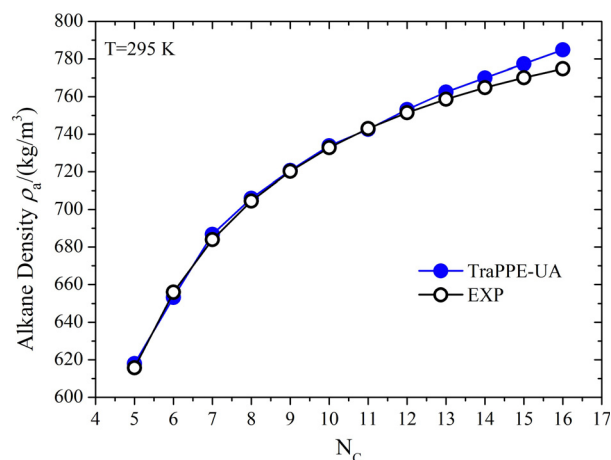


Fig. 2 Chain length (N_C) dependence of the bulk density values plotted for *n*-alkanes using the TraPPE-UA model (filled circles), compared with the values (open circles) extracted from the empirical equation of Olabisi and Simha.^{66,67}

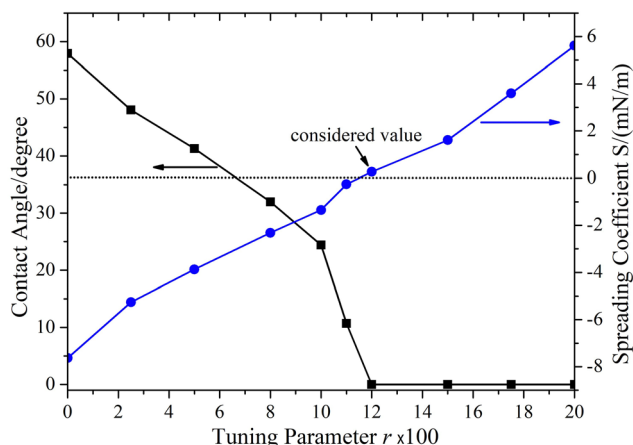


Fig. 3 Spreading coefficient and contact angle plotted versus the tuning parameter, r . This tuning parameter represents the interaction strength that is defined as $\epsilon_{OC} = (1+r)\sqrt{\epsilon_{O}\epsilon_{C}}$. The dotted line is a guideline for the zero spreading coefficient. Here, simulations are averaged over 50 ns.

and methylene groups after this tuning process are $\epsilon_{OC} = 0.88997$ and $\epsilon_{OC} = 0.609728$, respectively.

As shown in Fig. 3, increasing the interaction strength ϵ_{OC} by the factor $r = 0.12$ effectively enhances the water/*n*-alkane interfacial tensions at $T = 295$ K. Therefore, the new interaction strengths ϵ_{OC} significantly increased the spreading coefficient of heptane from -7.63 to 0.265 mN m^{-1} and decreased the contact angle from about 58° to 0° . This gives us a clear idea about the influential effects of the interaction strengths on the thermodynamic properties.^{24,25,70,71}

Our MD simulation results of TIP4P-2005/TraPPE-UA interfacial tensions are shown in Fig. 4. Fortunately, our results of water/*n*-alkane interfacial tension values have almost the same gradient as the experimental results. This confirms the validity of using $r = 0.12$ for all the *n*-alkane chains (*n*C5–*n*C16), and not just exclusively for heptane (*n*C7). The smooth behavior of the

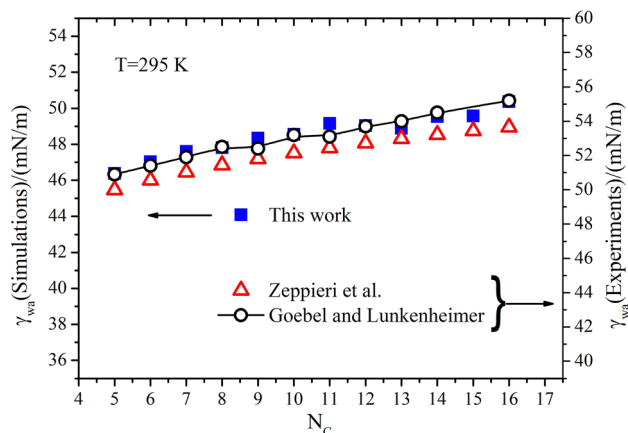


Fig. 4 Chain length (N_c) dependence of interfacial tension plotted for water/*n*-alkanes: TIP4P-2005/TraPPE-UA (squares) and compared with Goebel and Lunkenheimer¹ (open circles), and Zeppieri *et al.*² (open triangles) surface tension values. TraPPE-UA results are shifted up by 4.5 mN m^{-1} to compare with the experimental data.

Zeppieri *et al.* values is because they are calculated based on an empirical equation that was derived based on experimental data.² Their experimental data were correlated with an equation that depends only on the number of carbon atoms and the temperature to calculate the water/*n*-alkane interfacial tension. By contrast, the measurements by Goebel and Lunkenheimer are carried out under cumulative sequences of purification cycles on their samples, which makes their results more reliable.¹

In addition to the surface tension of pure *n*-alkanes (Fig. 1), we calculated the surface tension of TIP4P-2005 water at $T = 295$ K. The average surface tension of TIP4P-2005 water (averaged over 150 ns) is $\gamma_{\text{ww}} = 69.44$ mN m^{-1} , which is relatively close to the experimental value of 72.52 mN m^{-1} .⁷² Then, a set of MD simulations was carried out for water/*n*-alkane chains (*n*C5–*n*C16) with $r = 0.12$ at $T = 295$ K. Our simulation results were used to calculate the spreading coefficient and contact angle using eqn (1) and (3), respectively (shown in Fig. 5). Simulation results of the water/*n*-alkane contact angle and spreading coefficient show an impressive agreement with those calculated from the experimental data of Goebel and Lunkenheimer,¹ and they are also close to those calculated by Zeppieri *et al.*² Here, eqn (1) and (3) are, respectively, used to calculate the water/*n*-alkane spreading coefficient and contact angle using the experimental value of the water surface tension ($\gamma_{\text{ww}} = 72.52$ mN m^{-1}) and the experimental values of γ_{wa} and γ_{av} . Thus, there are two independent data sets to confirm the reliability of our MD simulations. These results of the spreading coefficients and contact angles demonstrate that the short *n*-alkanes (*n*C5–*n*C7) spread on the water surface initially, whereas a complete-to-partial initial wetting transition takes

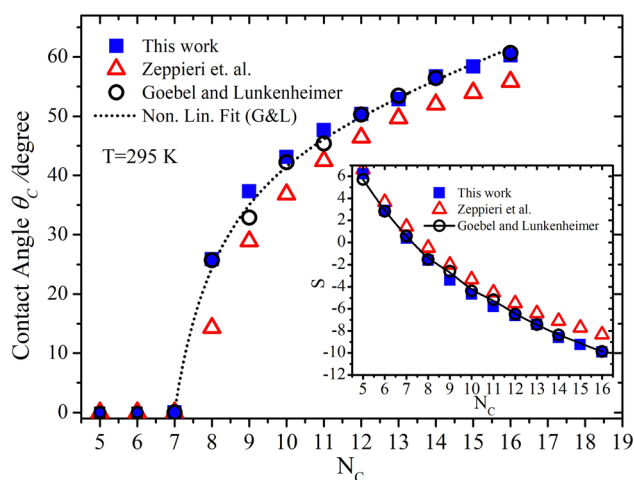


Fig. 5 Chain length (N_c) dependence of the contact angle plotted for water/*n*-alkanes using the TIP4P-2005/TraPPE-UA model (squares), compared with values based on data from Goebel and Lunkenheimer (open circles) and Zeppieri *et al.* (open triangles). Inset: The corresponding spreading coefficient is plotted vs. the *n*-alkane chain length using TIP4P-2005/TraPPE-UA (squares) and compared with data from Goebel and Lunkenheimer (open circles), and Zeppieri *et al.* (open triangles).^{1,2} The error bars are smaller than the symbols, and are not shown here. A table that includes these values is provided in the ESI.†

place as the *n*-alkane chain length grows (*n*C8–*n*C16). Indeed, this transition was expected at a fixed temperature because both the *n*-alkane/vapor and the water/*n*-alkane interfacial tensions increase with the chain length N_C . This means that the spreading coefficient, based on the definition in eqn (1), decreases with increasing N_C .[¶] This transition can be easily observed through the large jump in the contact angle from zero for heptane (*n*C7) to approximately 25° for octane (*n*C8), after which it then smoothly increases to around 60° for the hexadecane (*n*C16).

Since the water/vapor surface tension is constant at $T = 295$ K, the dramatic changes in the water/*n*-alkane wetting behavior must be driven by the water/*n*-alkane and *n*-alkane/vapor interfacial tensions. To view their effects on the spreading coefficient, we plotted the second term of eqn (1) (which we call $\gamma_{\text{sum}} = \gamma_{\text{wa}} + \gamma_{\text{av}}$) in a vertical plot (ladder plot), which makes the changes in its values more visible (see Fig. 6). Although the small *n*-alkane chains (*n*C5–*n*C7) wet the water surfaces completely, they have the largest variations in γ_{sum} . This observation indicates that the influence of increasing N_C is larger on the shorter *n*-alkanes (*n*C5–*n*C7) than on the longer ones (*n*C8–*n*C16). This could be because the short *n*-alkanes have a weaker tendency to orient parallel to the interface than do the longer chains, as we will discuss later. However, the value of γ_{sum} itself must exceed the water/vapor surface tension to have a transition to partial wetting. On other hand, the change in γ_{sum} between *n*C5 and *n*C16 ($\Delta\gamma_{\text{sum}} \approx 16.3 \text{ mN m}^{-1}$) is dominated by the change in the *n*-alkane/vapor surface tension $\Delta\gamma_{\text{av}} \approx 12.345 \text{ mN m}^{-1}$ while the change in the water/*n*-alkane interfacial tensions is only $\Delta\gamma_{\text{wa}} \approx 3.994 \text{ mN m}^{-1}$ (for comparison, water must be cooled from 295 to 210 K in order to, approximately, get 16 mN m^{-1} of change in the water/vapor surface tension). The spreading coefficient of heptane (*n*C7) is so close to the transition value ($S = 0 \text{ mN m}^{-1}$) that we can infer that the contact angle increases $\sim 29^\circ$ for a one carbon atom increase in chain length to octane (*n*C8), whereas it increases by less than 2° when moving from *n*C15 to *n*C16.

Since the magnitudes of γ_{sum} do not change equally with N_C (as shown in Fig. 6), this behavior invites us to investigate the effect of the water/*n*-alkane interface on the water and *n*-alkane molecules. The orientation of the water molecules and the hydrogen bond (HB) number in the water/*n*-alkane interface are qualitatively described by the charge density profile as shown in Fig. 7, where the Gibbs dividing surfaces (GDS) are located at $\rho_{\text{W}}(z) = \rho_{\text{A}}(z)$ and (whenever shown) shifted to $Z = 10 \text{ nm}$. Using the GROMACS package, the charge density profile is calculated by splitting the simulation box along the longitudinal axis into slices and thereby calculating the average charge in each slice. The charge density profiles at the water/(*n*C5–*n*C7) and water/(*n*C8–*n*C16) interfaces are different. For water/(*n*C5–*n*C7), the charge densities are relatively small and thus we have a lower degree of water orientation and a smaller

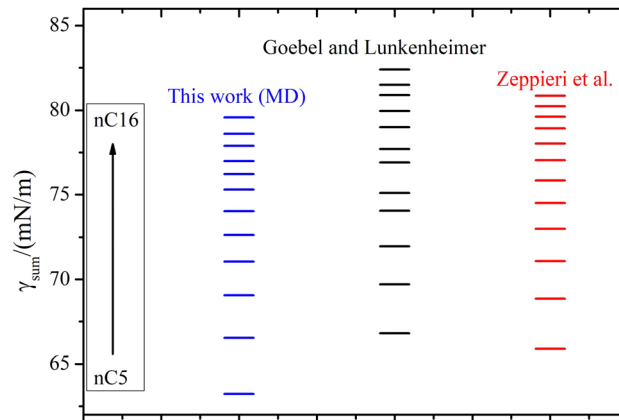


Fig. 6 Ladder plot of ($\gamma_{\text{sum}} = \gamma_{\text{wa}} + \gamma_{\text{av}}$) using the TIP4P-2005/TraPPE-UA model (left), compared with values based on data from Goebel and Lunkenheimer (middle) and Zeppieri *et al.* (right).^{1,2}

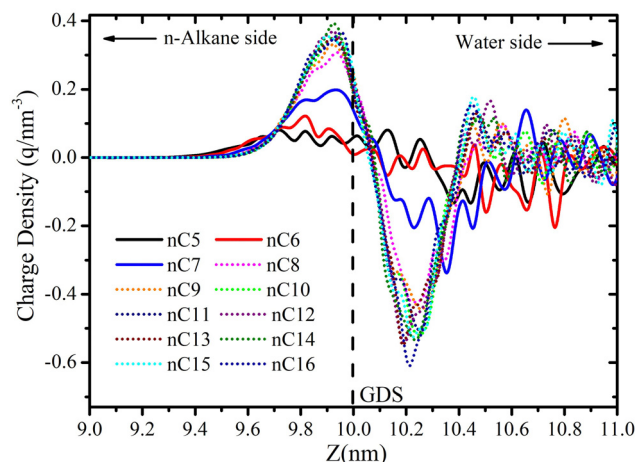


Fig. 7 Charge density profile of water plotted against the location in the interface, Z , normal to the water/*n*-alkane interface.

HB number. For the second group, water/(*n*C8–*n*C16), the sharper peaks of the charge densities indicate that the orientation of water molecules and the HB number are significantly boosted. This orientation creates two layers of charges in the interfaces (the outer one is positive and the inner one is negative). Because the number of neighboring water molecules available for HB is small in the interfaces, the water molecules orient preferentially to maximize the hydrogen bond number.³

The *n*-alkane chain length also has a significant effect on the interfacial water number density, as shown in Fig. 8. The water number density profiles also show a discontinuous change between the two groups, water/(*n*C5–*n*C7) and water/(*n*C8–*n*C16). The apophyses (the local maxima^{24,25,74,75}) are smaller and the interfaces are thicker for the shorter alkanes (*n*C5–*n*C7), whereas there is an abrupt increase in the water density (larger apophysis) accompanied by a decrease in the interface thickness for the second group, (*n*C8–*n*C16). The results shown in the Fig. 7 and 8 indicate that the effects of increasing the *n*-alkane chain size on water are similar to the effect of cooling the system.

[¶] Ragil *et al.* previously identified a temperature-dependent wetting transition of pentane on water. They experimentally observed the wetting transition temperature for pentane to be 53 °C.⁷³

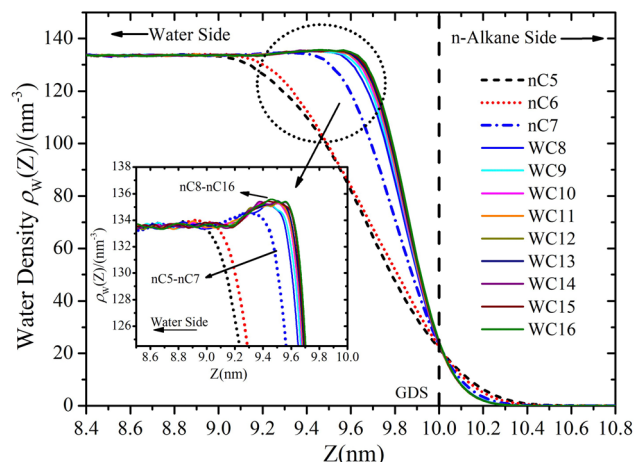


Fig. 8 Number density profile of water plotted against the location in the interface, Z , normal to the water/ n -alkane interface. Inset: Water density profiles near the water/ n -alkane interface.

Further investigations were performed to assess the effects of water/ n -alkane interfaces on the n -alkane density. Apparently, as shown in Fig. 9, these effects are long-range, manifesting as interfacial layering structures that extend deep into the (n C8– n C16) bulk liquid n -alkane. We also see the dramatic complete-to-partial initial wetting transition in terms of the interfacial thicknesses t , as shown in the inset of Fig. 9. The interfacial thickness t represents the interfacial region in the density profile where the density changes from 10% ($z_{10\%}$) to 90% ($z_{90\%}$) of the average bulk liquid density ρ_l . The interfaces are thicker for (n C5– n C7) and thinner for (n C8– n C16). These observations confirm that the behavior of the water/ n -alkane interfaces with increasing n -alkane chain length is similar to cooling, *i.e.*, lower temperatures result in thinner interfaces. It is worth mentioning here that the interface thickness values are inversely proportional to the interfacial

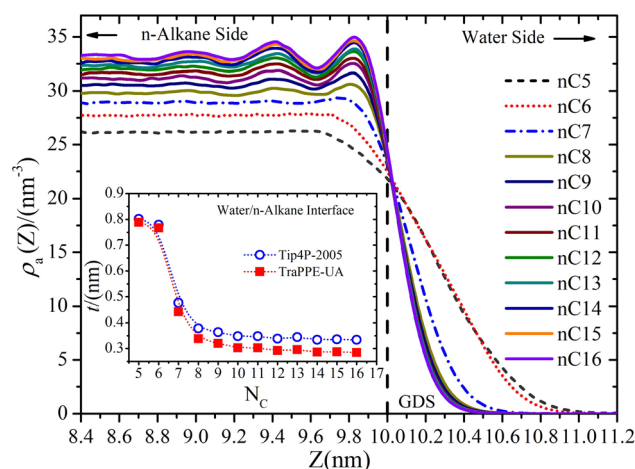


Fig. 9 Density profiles for n -alkane in the water/ n -alkane interface plotted against the location in the interface, Z , normal to the water/ n -alkane interface. Inset: Interface thickness of water (open circles) and n -alkane (squares), as shown in Fig. 8, versus the n -alkane chain length N_c .

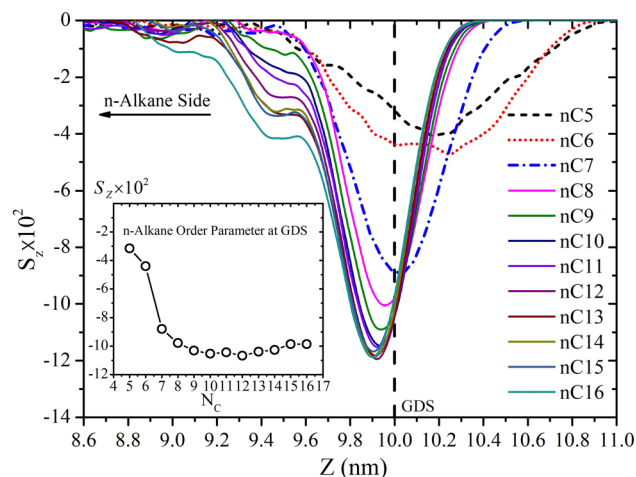


Fig. 10 Orientational order parameter (S_z) of n -alkane molecules in the water/ n -alkane interfaces plotted against the location in the interface, Z , normal to the water/ n -alkane interface. Inset: Orientation order parameter at the Gibbs dividing surface (all shifted to $Z = 10$ nm) versus the n -alkane chain length N_c .

tension values, in agreement with the theoretical prediction, $t^2 \approx \gamma^{-1.23,76,77}$.

We also calculated the n -alkane molecular orientation in terms of the order parameter S_z at the water/ n -alkane interface. As shown in Fig. 10, the layered n -alkane interfaces (for n C8– n C16) are indicated by the meandering behavior of the order parameter S_z to the left of the Gibbs dividing surface (GDS). An interesting observation is that the minimum S_z values of the short n -alkanes (n C5– n C7) are on the water side of the water/ n -alkane interface (to the right of GDS) while those of the longer n -alkanes (n C8– n C16) are on the n -alkane side of the interfaces (to the left of the GDS). In terms of the molecular orientation, this observation is consistent with the results of the water and n -alkane interfacial thicknesses (inset of Fig. 9) where the shorter n -alkanes have a weaker tendency to orient parallel to the interface; hence, they have a greater mutual interfacial penetration with water (Fig. 11(a)) while the longer n -alkanes have less mutual penetration (Fig. 11(b)). The order parameter at the GDS is shown in the inset of Fig. 10 where a rapid decline occurs at the complete-to-partial initial wetting transition. This behavior is consistent with our results of the

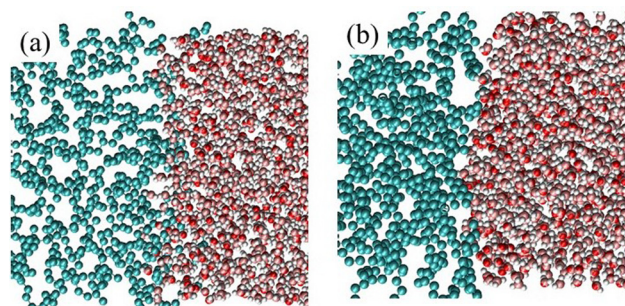


Fig. 11 Snapshots of water/ n -alkane interfaces (side view): (a) water/ n C5 and (b) water/ n C16.

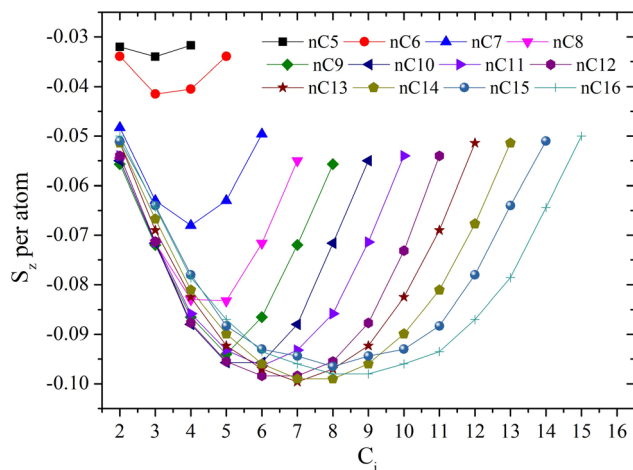


Fig. 12 Orientational order parameter (S_z) per atom of n -alkane molecules in the water/ n -alkane interfaces at the Gibbs dividing surface (GDS) plotted against the atom index C_i (for atom i , atoms $i - 1$ and $i + 1$ are used to calculate $S_z(C_i)$).⁷⁸

contact angle and spreading coefficient, demonstrating that the complete-to-partial initial wetting transition of water/ n -alkane systems occurs upon increasing the n -alkane chain length.

In addition to the moderate increase in alkane ordering for the larger alkanes at the interface, we noted several effects on the molecular conformation of n -alkanes at the interface using the orientational order parameter per atom (explained in the caption of Fig. 12). As shown in Fig. 12, n -alkane molecules form a nearly “horseshoe” or “C-shaped” structure that is symmetric about the central segments. The curving of the n -alkane molecules increases as their length increase, and they also become more parallel to the interface. The central segments of the n -alkane molecules are more parallel to the interface than the end segments. This can be understood since the “horseshoe” structure of the n -alkane molecules is not

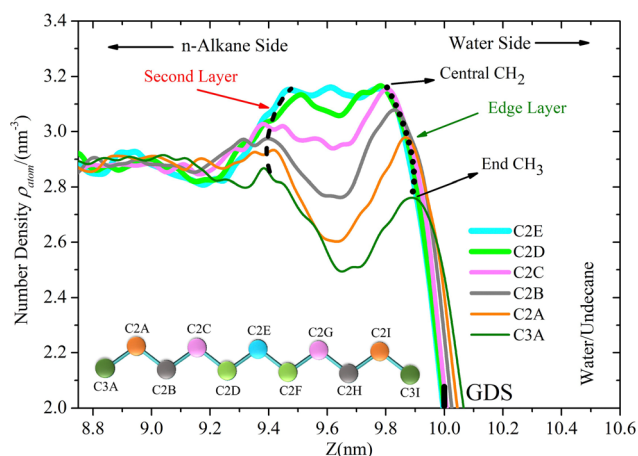


Fig. 13 Number density profiles of undecane ($nC11$) atoms plotted against the location Z , normal to the water/ n -alkane interface. Thick dotted and dashed lines show half of the molecular conformation of undecane (side view) in the outer layer (right) and the second layer (left), respectively.

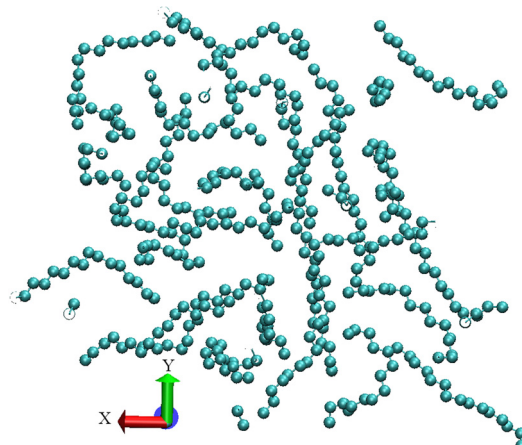


Fig. 14 Snapshot of n -alkane molecules in the water/ $nC16$ interface.

exactly parallel to the interface but is rotated slightly about the central segments so the end segments are either closer to water or farther away.

To make our results of the molecular conformation more visible, as shown in Fig. 13, we calculated the atomic density profiles of undecane, as an example. The undecane atoms are labeled as C3A–C3I and C2A–C2I, respectively, for the methyl and methylene groups, where the central segment is indexed as C2E. We show only half of the density profiles because they are symmetric about C2E. The peaks show that the density of the central segment (C2E) is the highest while the density of the end segment (C3A) is the lowest. This confirms that the edges of the “horseshoe” or “C-shaped” structure in the outer layer are closer to the water.

Using the 3D visual molecular dynamics (VMD) software,⁷⁹ Fig. 14 shows, as an example, a snapshot of the n -alkane molecules in the water/ $nC16$ interface. We see that the majority of the molecules have a “horseshoe” or “C-shaped” structure. Hence, we can consider this observation as a visual confirmation of the “horseshoe” or “C-shaped” geometry to be the average structure of n -alkane molecules in the water/ n -alkane interfaces, particularly for $nC8$ – $nC16$.

4 Conclusions

We have studied the surface tension of n -alkane systems ($nC5$ to $nC16$) using molecular dynamics simulations. We used two united atom models in this study: the PYS and TraPPE-UA force fields. The PYS results do not correspond well with the carbon-number behavior of the n -alkane surface tension found by Goebel and Lunkenheimer,¹ whereas the TraPPE-UA results do. Thus, we concentrate on the TraPPE-UA force field in this work. The corresponding water/ n -alkane interfacial tension values are calculated at $T = 295$ K and used in calculating the spreading coefficient and contact angles of these n -alkanes on water. Water is modeled with the TIP4P-2005 force field and its simulated value of surface tension is 69.437 mN m^{-1} at $T = 295$ K. A parameter $r = 0.12$ is used to tune the water/ n -alkane interaction strength $\epsilon_{OC} = (1 + r)\sqrt{\epsilon_{O^*} \epsilon_C}$ to reproduce

the wetting behavior of water/heptane ($nC7$) at $T = 295$ K. Our results for the spreading coefficients and contact angles of water/ n -alkane systems (with $r = 0.12$) agree very well with experimental results (calculated using the results of Goebel and Lunkenheimer, and those of Zeppieri *et al.*).^{1,2} They also agree with older estimates of the initial spreading coefficients, indicating that the smaller alkanes should all initially wet water perfectly.⁸⁰ For short n -alkane molecules, the sum of the interfacial tension values of water/ n -alkane and n -alkane/vapor (represented by γ_{sum}) is small and thus the complete wetting regime is energetically favorable. It is worth mentioning here that this sum of interfacial tension values is dominated by the n -alkane/vapor interfacial tension. With increasing n -alkane chain length N_C , our results, in agreement with experimental values of surface tension, show a faster increase in the n -alkane/vapor tension than in the water/ n -alkane interfacial tension. Heptane ($nC7$) is the longest n -alkane that, at least initially, completely wets water at $T = 295$ K. Starting from octane ($nC8$ – $nC16$), γ_{sum} becomes larger than that of water/vapor, γ_{wv} . This prevents the complete wetting mode from minimizing the surface free energy. Thus, in order to decrease the total surface free energy, n -alkane starts partially dewetting the water surface. This creates three-interface systems (water/ n -alkane, water/vapor, and n -alkane/vapor). This partial dewetting reaches an equilibrium state when the three tensions satisfy the relations of Neumann's triangle in which the contact angle increases with increasing γ_{sum} (or increases with N_C).²³

Furthermore, we investigated the effects of complete-to-partial initial wetting transitions on several interfacial properties. We have found that the thicknesses of the n -alkane/water interfaces show a strong decrease near this transition but barely vary for the larger n -alkanes. The water density increases in the water/ n -alkane interface with increasing n -alkane size, and it is accompanied by the molecular re-orientation of water, leading to an increase in the number of hydrogen bonds.³ We investigated this re-orientation by calculating the average charge density along the normal-to-interface director. At the complete-to-partial initial wetting transition, the n -alkane liquid phases near the water/ n -alkane interfaces are transformed from relatively homogeneous bulk phases ($nC5$ – $nC7$) to layered structures ($nC8$ – $nC16$). The orientation of the n -alkane molecules is explored using an orientational order parameter S_z . The n -alkanes are laterally oriented in the water/ n -alkane interface, which ensures that most of the length of the n -alkane is in close contact with the water.^{3,81} Our results show that the larger the n -alkane molecules are, the more parallel to the interface they are.

The conformation of the n -alkane molecules is quantitatively investigated by calculating the order parameter per atom $C_i = 2 \cdot \langle S_z \rangle \cdot (N_C - 1)$. Our results show that the central segments are more laterally oriented than the end segments. This indicates that the n -alkane molecules are not linear but that they systematically curve into "horseshoe" or "C-shaped" structures. To observe how the end segments of the n -alkane molecules orient with respect to the water surface, we calculated the density profiles of individual n -alkane atoms. We found that the

densities of the central atoms are maximized and that the density decreases systematically for atoms farther from the chain center. We also observed that the end segments are slightly closer to the water in the outer layer of n -alkane.

In summary, we can say that the main implication of our work is that the initial wetting state (complete or partial) seems to be reflected in the differences found in the water/ n -alkane interfacial structure.

Conflicts of interest

There are no conflicts to declare.

Acknowledgements

We gratefully acknowledge the assistance of Prof. Thomas Vojta in using the Pegasus IV computer cluster in the Physics Department at Missouri S&T. Computational work was also performed using the Foundry HPC supported by the National Science Foundation under grant no. OAC-1919789.

Notes and references

- 1 A. Goebel and K. Lunkenheimer, *Langmuir*, 1997, **13**, 369–372.
- 2 S. Zeppieri, J. Rodríguez and A. L. López de Ramos, *J. Chem. Eng. Data*, 2001, **46**, 1086–1088.
- 3 H. Xiao, Z. Zhen, H. Sun, X. Cao, Z. Li, X. Song, X. Cui and X. Liu, *Sci. China: Chem.*, 2010, **53**, 945–949.
- 4 D. M. Mitrović, A. M. Tikhonov, M. Li, Z. Huang and M. L. Schlossman, *Phys. Rev. Lett.*, 2000, **85**, 582.
- 5 T. R. Underwood and H. C. Greenwell, *Sci. Rep.*, 2018, **8**, 352.
- 6 F. G. Moore and G. L. Richmond, *Acc. Chem. Res.*, 2008, **41**, 739–748.
- 7 M. Natália and D. S. Cordeiro, *Mol. Simul.*, 2003, **29**, 817–827.
- 8 R. E. Johnson and R. H. Dettre, *J. Colloid Interface Sci.*, 1966, **21**, 610–622.
- 9 F. Hauxwell and R. H. Ottewill, *J. Colloid Interface Sci.*, 1970, **34**, 473–479.
- 10 P. Richmond, B. W. Ninham and R. H. Ottewill, *J. Colloid Interface Sci.*, 1973, **45**, 69–80.
- 11 C. Del Cerro and G. J. Jameson, *J. Colloid Interface Sci.*, 1980, **78**, 362–375.
- 12 T. Takii and Y. H. Mori, *J. Colloid Interface Sci.*, 1993, **161**, 31–37.
- 13 S.-Y. Akatsuka, H. Yoshigiwa and Y. H. Mori, *J. Colloid Interface Sci.*, 1995, **172**, 335–340.
- 14 K. Ragil, D. Bonn, D. Broseta and J. Meunier, *J. Chem. Phys.*, 1996, **105**, 5160–5167.
- 15 D. Thanh-Khac Pham and G. J. Hirasaki, *J. Pet. Sci. Eng.*, 1998, **20**, 239–246.
- 16 T. Pföhl and H. Riegler, *Phys. Rev. Lett.*, 1999, **82**, 783–786.
- 17 E. Bertrand, D. Bonn, J. Meunier and D. Segal, *Phys. Rev. Lett.*, 2001, **86**, 3208.

- 18 O.-S. Kwon, H. Jing, K. Shin, X. Wang and S. K. Satija, *Langmuir*, 2007, **23**, 12249–12253.
- 19 N. Shahidzadeh, D. Bonn, K. Ragil, D. Broseta and J. Meunier, *Phys. Rev. Lett.*, 1998, **80**, 3992–3995.
- 20 E. Bertrand, H. Dobbs, D. Broseta, J. Indekeu, D. Bonn and J. Meunier, *Phys. Rev. Lett.*, 2000, **85**, 1282–1285.
- 21 V. C. Weiss and B. Widom, *Phys. A*, 2001, **292**, 137–145.
- 22 V. C. Weiss, *J. Chem. Phys.*, 2006, **125**, 084718.
- 23 J. S. Rowlinson and B. Widom, *Molecular Theory of Capillarity*, Dover Publications, 2002.
- 24 P. Neupane and G. Wilemski, *Phys. Chem. Chem. Phys.*, 2021, **23**, 14465–14476.
- 25 Y. Qiu and V. Molinero, *Crystals*, 2017, **7**, 86.
- 26 R. Mohammadi, J. Wassink and A. Amirfazli, *Langmuir*, 2004, **20**, 9657–9662.
- 27 Y. Wu, P. J. Shuler, M. Blanco, Y. Tang and W. A. Goddard, SPE/DOE Symposium on Improved Oil Recovery, 2006.
- 28 T. Schneider and E. Stoll, *Phys. Rev. B: Solid State*, 1978, **17**, 1302–1322.
- 29 K. Lunkenheimer and K. D. Wantke, *J. Colloid Interface Sci.*, 1978, **66**, 579–581.
- 30 P.-L. Chau and A. J. Hardwick, *Mol. Phys.*, 1998, **93**, 511–518.
- 31 J. G. Harris, *J. Phys. Chem.*, 1992, **96**, 5077–5086.
- 32 N. Waheed, M. J. Ko and G. C. Rutledge, *Polymer*, 2005, **46**, 8689–8702.
- 33 N. Waheed, M. S. Lavine and G. C. Rutledge, *J. Chem. Phys.*, 2002, **116**, 2301–2309.
- 34 W. Paul, D. Y. Yoon and G. D. Smith, *J. Chem. Phys.*, 1995, **103**, 1702–1709.
- 35 M. G. Martin and J. I. Siepmann, *J. Phys. Chem. B*, 1998, **102**, 2569–2577.
- 36 S. J. Keasler, S. M. Charan, C. D. Wick, I. G. Economou and J. I. Siepmann, *J. Phys. Chem. B*, 2012, **116**, 11234–11246.
- 37 K. A. Maerzke, N. E. Schultz, R. B. Ross and J. I. Siepmann, *J. Phys. Chem. B*, 2009, **113**, 6415–6425.
- 38 L. Zhang and J. I. Siepmann, *J. Phys. Chem. B*, 2005, **109**, 2911–2919.
- 39 V. P. Modak, H. Pathak, M. Thayer, S. J. Singer and B. E. Wyslouzil, *Phys. Chem. Chem. Phys.*, 2013, **15**, 6783–6795.
- 40 A. J. Bourque, C. R. Locker and G. C. Rutledge, *J. Phys. Chem. B*, 2017, **121**, 904–911.
- 41 A. Bourque, C. R. Locker and G. C. Rutledge, *Macromolecules*, 2016, **49**, 3619–3629.
- 42 P. Yi and G. C. Rutledge, *J. Chem. Phys.*, 2009, **131**, 134902.
- 43 P. Yi and G. C. Rutledge, *J. Chem. Phys.*, 2011, **135**, 024903.
- 44 F. Hrahsheh and G. Wilemski, *AIP Conf. Proc.*, 2013, **1527**, 63–66.
- 45 T. Yamamoto, *Polymer*, 2016, **99**, 721–733.
- 46 A. Obeidat, F. Hrahsheh and G. Wilemski, *J. Phys. Chem. B*, 2015, **119**, 9304–9311.
- 47 F. Hrahsheh, Y. S. Wudil and G. Wilemski, *Phys. Chem. Chem. Phys.*, 2017, **19**, 26839–26845.
- 48 J. L. F. Abascal and C. Vega, *J. Chem. Phys.*, 2005, **123**, 234505.
- 49 C. Vega and E. de Miguel, *J. Chem. Phys.*, 2007, **126**, 154707.
- 50 J. Alexandre and G. A. Chapela, *J. Chem. Phys.*, 2010, **132**, 014701.
- 51 J. M. Míguez, D. González-Salgado, J. L. Legido and M. M. Piñeiro, *J. Chem. Phys.*, 2010, **132**, 184102.
- 52 R. Sakamaki, A. K. Sum, T. Narumi and K. Yasuoka, *J. Chem. Phys.*, 2011, **134**, 124708.
- 53 D. Van Der Spoel, E. Lindahl, B. Hess, G. Groenhof, A. E. Mark and H. J. C. Berendsen, *J. Comput. Chem.*, 2005, **26**, 1701–1718.
- 54 B. Hess, C. Kutzner, D. van der Spoel and E. Lindahl, *J. Chem. Theory Comput.*, 2008, **4**, 435–447.
- 55 S. Páll, A. Zhmurov, P. Bauer, M. Abraham, M. Lundborg, A. Gray, B. Hess and E. Lindahl, *J. Chem. Phys.*, 2020, **153**, 134110.
- 56 M. J. Abraham, T. Murtola, R. Schulz, S. Páll, J. C. Smith, B. Hess and E. Lindahl, *SoftwareX*, 2015, **1**, 19–25.
- 57 W. C. Swope, H. C. Andersen, P. H. Berens and K. R. Wilson, *J. Chem. Phys.*, 1982, **76**, 637–649.
- 58 G. Bussi, D. Donadio and M. Parrinello, *J. Chem. Phys.*, 2007, **126**, 014101.
- 59 B. Hess, H. Bekker, H. J. C. Berendsen and J. G. E. M. Fraaije, *J. Comput. Chem.*, 1997, **18**, 1463–1472.
- 60 T. Darden, D. York and L. Pedersen, *J. Chem. Phys.*, 1993, **98**, 10089–10092.
- 61 N. M. Fischer, P. J. van Maaren, J. C. Ditz, A. Yildirim and D. van der Spoel, *J. Chem. Theory Comput.*, 2015, **11**, 2938–2944.
- 62 U. Essmann, L. Perera, M. L. Berkowitz, T. Darden, H. Lee and L. G. Pedersen, *J. Chem. Phys.*, 1995, **103**, 8577–8593.
- 63 C. L. Wennberg, T. Murtola, B. Hess and E. Lindahl, *J. Chem. Theory Comput.*, 2013, **9**, 3527–3537.
- 64 P. J. in't Veld, A. E. Ismail and G. S. Grest, *J. Chem. Phys.*, 2007, **127**, 144711.
- 65 R. Toutouni, J. Kubelka and M. Piri, *J. Phys. Chem. B*, 2021, **125**, 6658–6669.
- 66 O. Olabisi and R. Simha, *J. Appl. Polym. Sci.*, 1977, **21**, 149–163.
- 67 S. K. Nath, J. D. McCoy and J. G. Curro, *Macromolecules*, 1995, **28**, 3275–3281.
- 68 H. A. Lorentz, *Ann. Phys.*, 1881, **248**, 127–136.
- 69 D. Berthelot, *C. R. Acad. Sci.*, 1898, **126**, 1703–1855.
- 70 F. Hrahsheh, *Fluid Phase Equilib.*, 2019, **501**, 112272.
- 71 T. Morawietz, A. Singraber, C. Dellago and J. Behler, *Proc. Natl. Acad. Sci. U. S. A.*, 2016, **113**, 8368–8373.
- 72 N. B. Vargaftik, B. N. Volkov and L. D. Voljak, *J. Phys. Chem. Ref. Data*, 1983, **12**, 817–820.
- 73 K. Ragil, D. Bonn, D. Broseta, J. Indekeu, F. Kalaydjian and J. Meunier, *J. Pet. Sci. Eng.*, 1998, **20**, 177–183.
- 74 V. P. Modak, B. E. Wyslouzil and S. J. Singer, *J. Chem. Phys.*, 2020, **153**, 224501.
- 75 X. Wang, K. Binder, C. Chen, T. Koop, U. Pöschl, H. Su and Y. Cheng, *Phys. Chem. Chem. Phys.*, 2019, **21**, 3360–3369.
- 76 S. Senapati and M. L. Berkowitz, *Phys. Rev. Lett.*, 2001, **87**, 176101.
- 77 A. Das and S. M. Ali, *J. Mol. Liq.*, 2019, **277**, 217–232.
- 78 J. Fu and S. G. Urquhart, *Langmuir*, 2007, **23**, 2615–2622.
- 79 W. Humphrey, A. Dalke and K. Schulten, *J. Mol. Graphics*, 1996, **14**, 33–38.
- 80 H. Dobbs and D. Bonn, *Langmuir*, 2001, **17**, 4674–4676.
- 81 G. Rucker, X. Yu and L. Zhang, *Fuel*, 2020, **267**, 117252.